Electronic Supplementary Material (ESI) for Journal of Materials Chemistry C.

Supporting Information

A multifunctional flexible sensor with coupling bionic microstructures inspired by nature

Linpeng Liu[a], *Xiancun Meng*[b], *Changchao Zhang*[b], *You Chen*[b], *Tao Sun*[b], *Zhilai Lu*[a], *Junqiu Zhang*[b], *Shichao Niu*[b], *Zhiwu Han*[b], and *Ji-An Duan*[a]

[a] The State Key Laboratory of High Performance and Complex Manufacturing, College of Mechanical and Electrical Engineering, Central South University, Changsha 410012, China

[b] Key Laboratory of Bionic Engineering, Ministry of Education, Jilin University, Changchun 130022, China

Corresponding Authors

*Shichao Niu: niushichao@jlu.edu.cn

*Zhiwu Han: zwhan@jlu.edu.cn

*Ji-An Duan: duanjian@csu.edu.cn

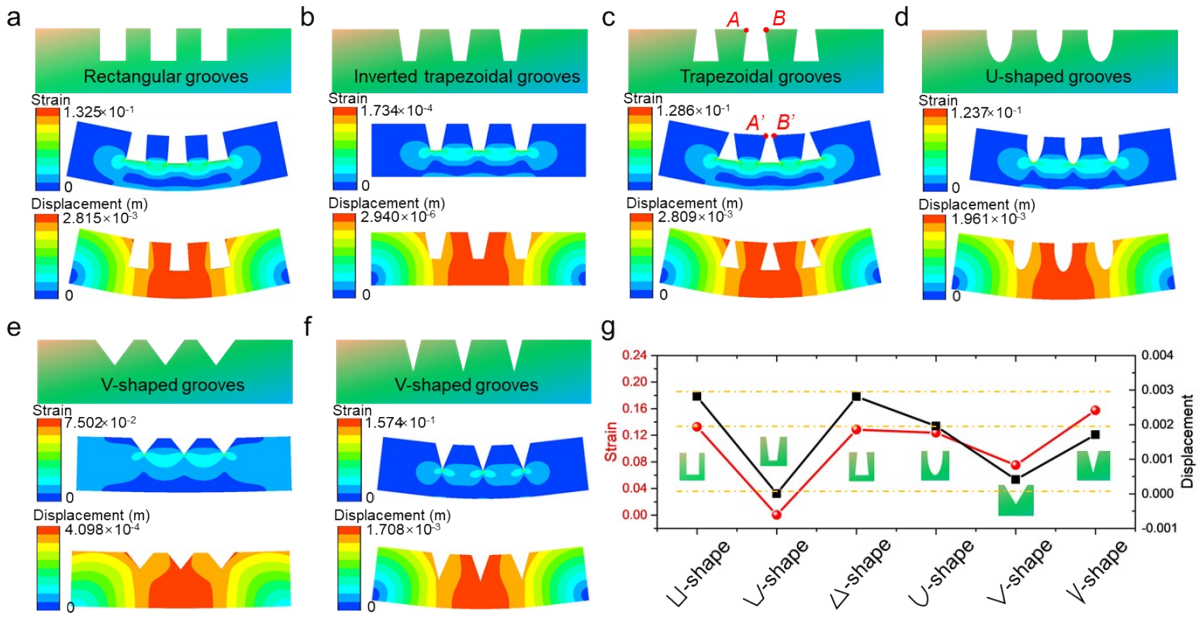

Fig. S1. Finite Element Analysis (FEA) for grooves with different cross sectional geometries. The models used for FEA have a same size with a length of 40 mm, a width of 20 mm and a height of 10 mm. And the grooves with different cross sectional shapes have a uniform length of 40 mm and a height of 5 mm. The crucial properties of the material used for simulation were set as a density of 1.2 Kg m^{-3}, a Young's Modulus of 2.5 Mpa, a Poisson's Ratio of 0.35. And the applied pressure load was 0.02 Mpa, from the left and right sides of the model. (a) FEA for grooves with a rectangular shape, the width of each groove is 4 mm. (b) FEA for grooves with an inverted trapezoidal shape, the width of the top and bottom of each groove is 4 mm and 2 mm, respectively. (c) FEA for grooves with a trapezoidal shape, the width of the top and bottom of each groove is 2 mm and 4 mm, respectively. (d) FEA for grooves with a U shape, the width of each groove is 4 mm. (e) FEA for grooves with a V shape, the opening angle of each groove is ~80°. (f) FEA for grooves with a V shape, the opening angle of each groove is ~45°. (g) A comparison of FEA results for grooves with different cross-sectional geometries regarding the strain and displacement (the distance change of points A and B), shows that the V-shaped groove with an acute angle has a larger strain than others, which could be better for the design of strain sensor.

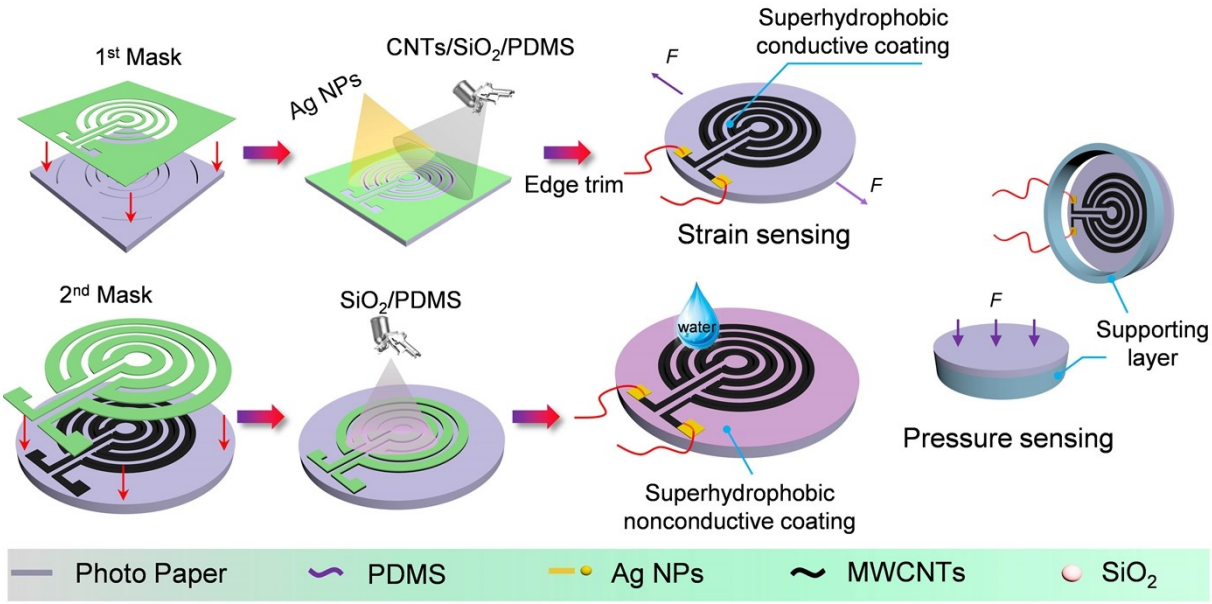

Fig. S2. Schematic illustration for the preparation process of the bionic paper-based sensor with strain and pressure sensing capacity and superhydrophobic property.

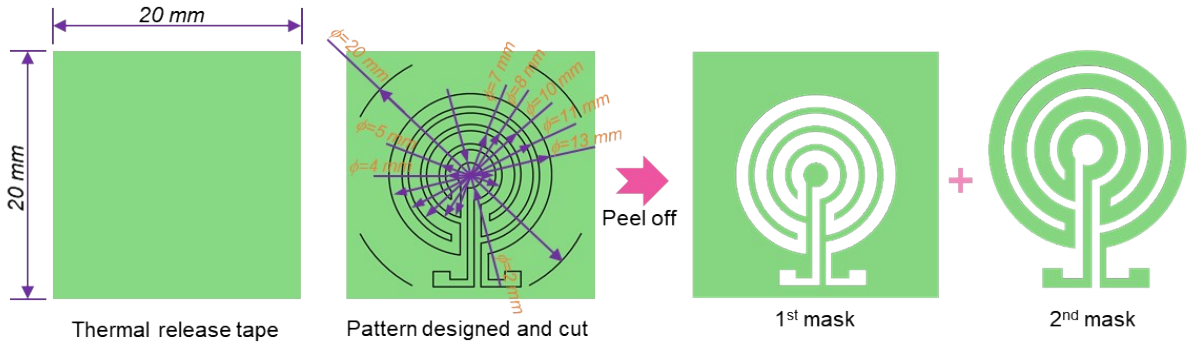

Fig. S3. The design of groove pattern and the fabricating process of the masks.

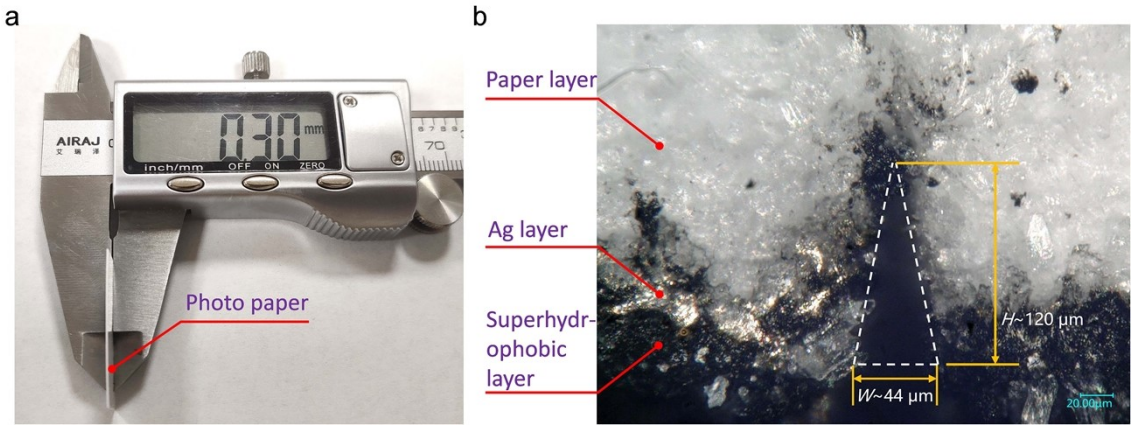

Fig. S4. (a) The thickness of the photo paper, showing the paper material has a thickness of ~300 μm. (b) The cross section of the bionic paper-based sensor, showing the V-shaped groove has a depth of ~120 μm, while the width of the groove is around 44 μm.

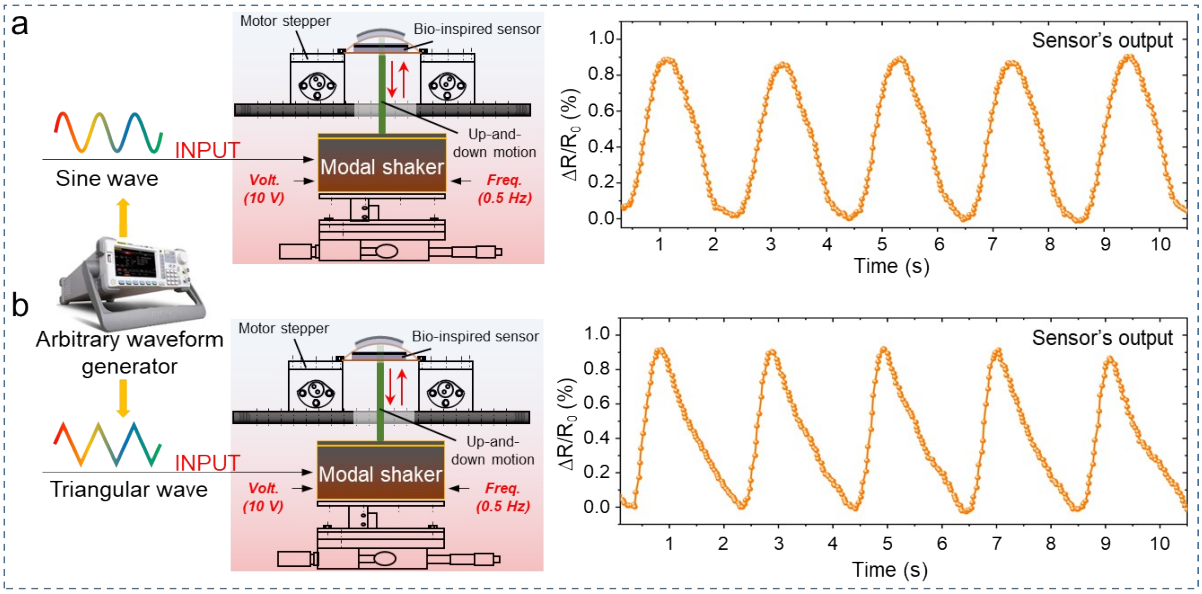

Fig. S5. The responses of the bioinspired paper-based sensors to different waveforms input. (a) The relative resistance change of the sensor as a function of time. An arbitrary waveform generator generated sine wave with a voltage of 10 V (a bending strain of ~0.03%) and a frequency of 0.5 Hz and then input to the modal shake to load stimuli to the sensor. (b) The relative resistance change of the sensor as a function of time. An arbitrary waveform generator generated triangular wave with a voltage of 10 V (a bending strain of ~0.03%) and a frequency of 0.5 Hz and then input to the modal shake to load stimuli to the sensor. All results show that the sensor has a similar output with the waveforms input, that is, the sensor has a waveform recognition capability.

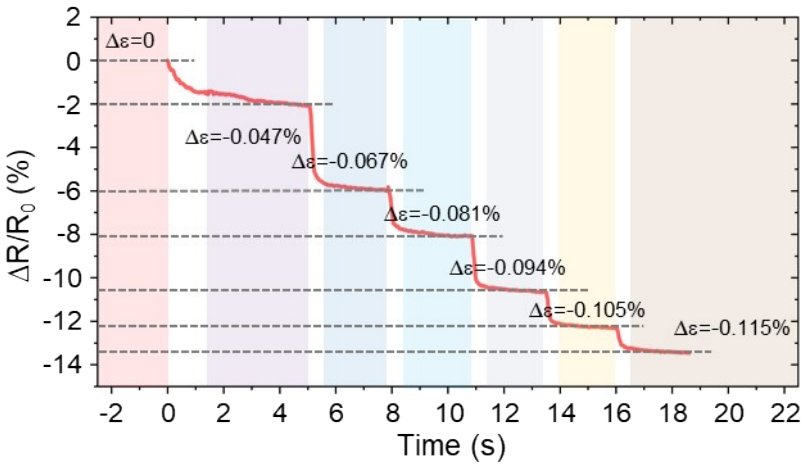

Fig. S6. The response of sensor under different compressive strains. The strain was applied incrementally in a stepwise way.

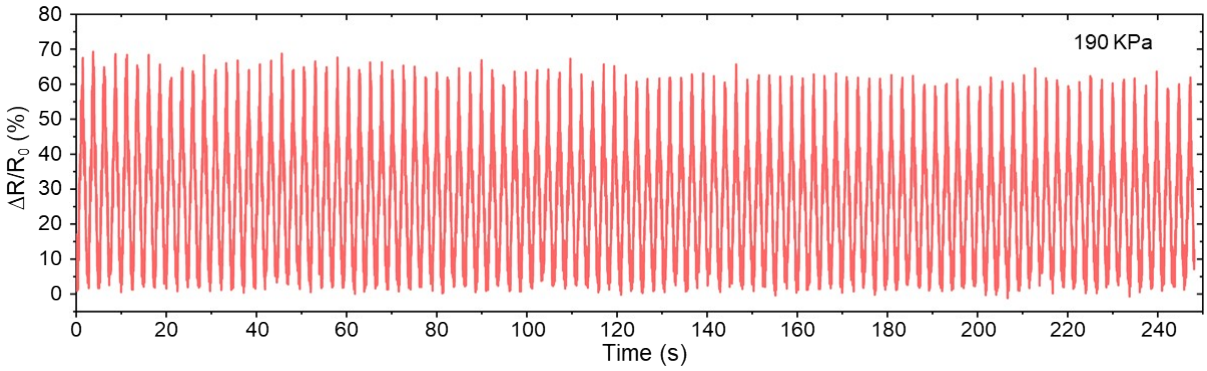

Fig. S7. The relative resistance change of the paper-based sensor serving as a pressure sensor under an applied pressure of 190 kPa.

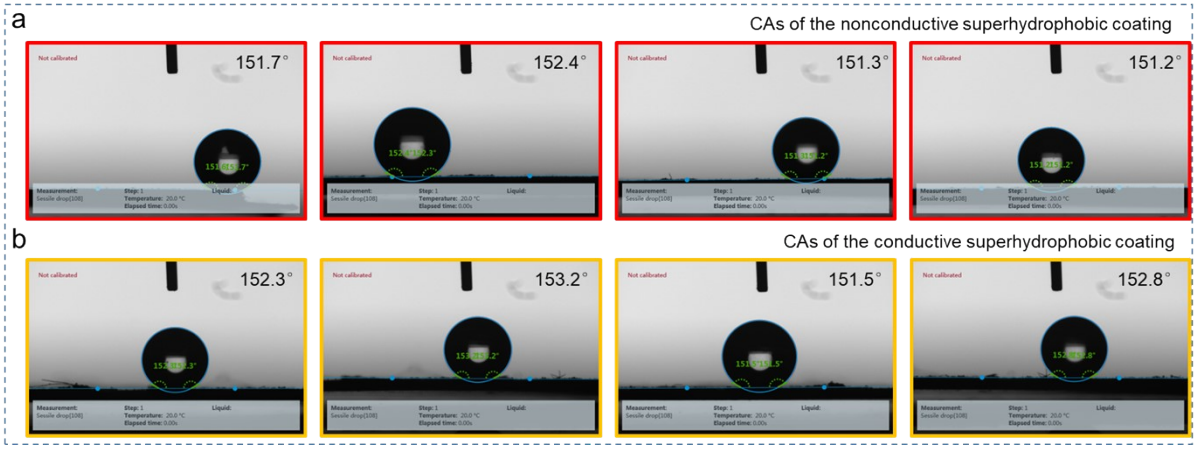

Fig. S8. The water contact angles of the nonconductive superhydrophobic coating and the conductive superhydrophobic coating. **(**a) The water contact angles of the nonconductive superhydrophobic coating at different locations, showing an average angle of 151.2°. **(**b) The water contact angles of the conductive superhydrophobic coating at different locations, showing an average angle of 152.3°.

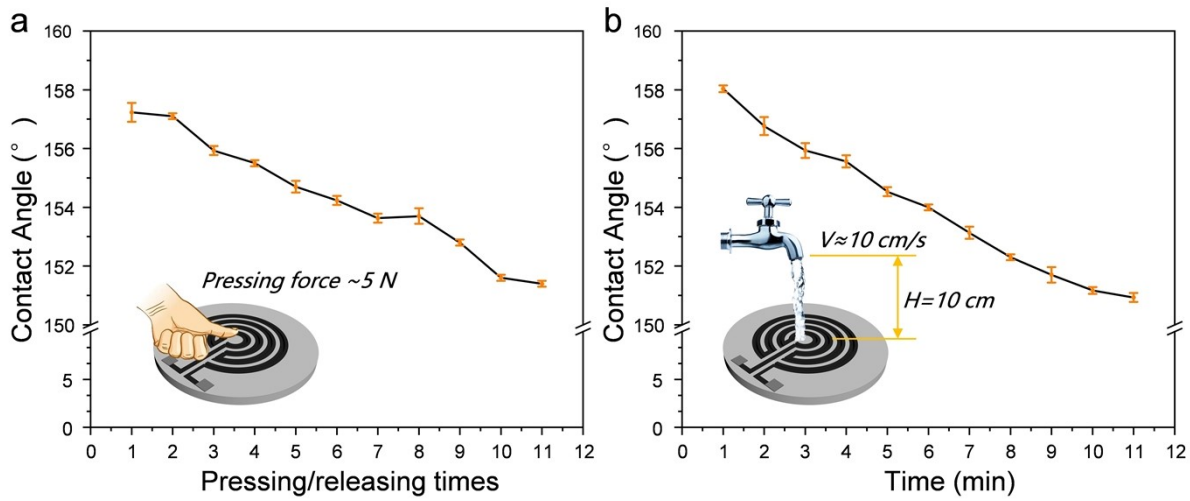

Fig. S9. Robustness test of the bioinspired paper-based sensor. (a) Variation of CA under the finger press. (b) Variation of CA under water flow test. The inset shows the schematic diagram of the corresponding test.

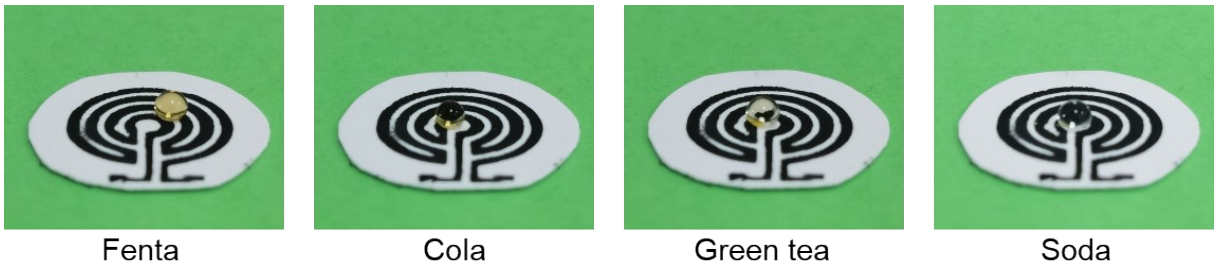

Fig. S10. Pictures of the droplets of liquid on the surface of the sensor, including fenta, cola, green tea and soda are spherical in shape on the sensor surface.

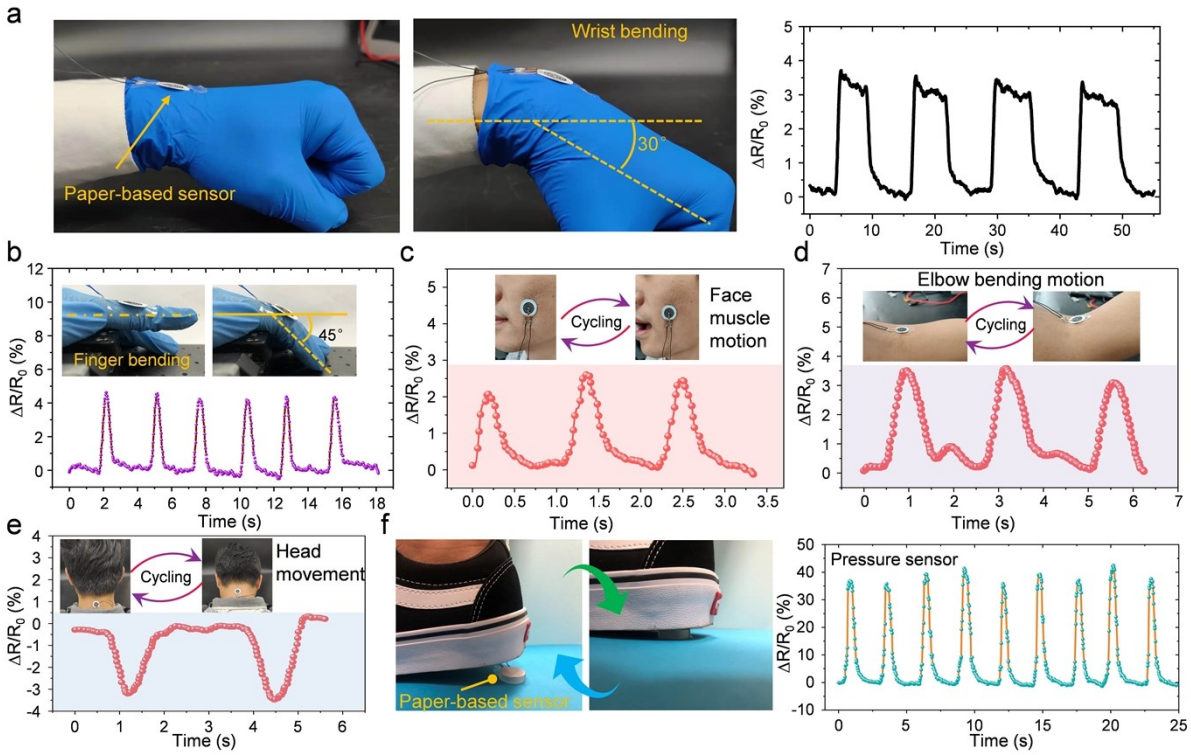

Fig. S11. The paper-based sensor serves as a strain sensor to monitor the motions of human muscles and joints. (a) Application of the paper-based sensor serving as a strain sensor for monitoring the movement of wrist with a bending angle of 30°. (b) The paper-based sensor used to detect the finger motion bending at an angle of ~45°. (c) The paper-based sensor used to detect the face muscle motion. The sensor was attached to the face of an adult volunteer. (d) The paper-based sensor used to detect the elbow bending motion. (e) The paper-based sensor used to detect head movement. The sensor was attached to the neck of an adult volunteer. (f) Response curves of the paper-based sensor served as a pressure sensor for monitoring the footstep movement of a 55 Kg adult.

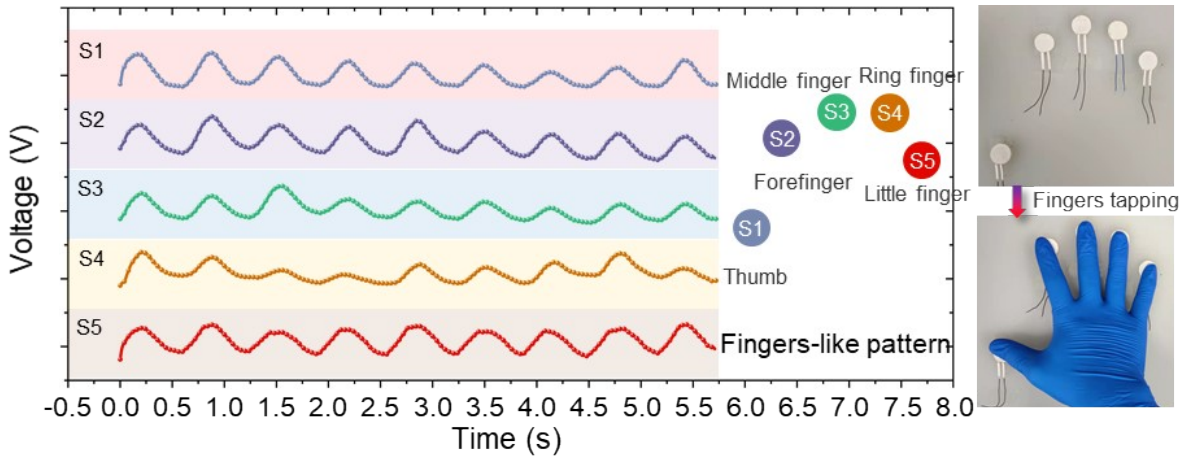

Fig. S12. The responses of sensors arrayed in a fingers-like pattern to the fingers tapping motions, showing that the 5 pressure sensors have consistent responses to the tapping motions, which represents that the sensor could be used as a touch sensor.

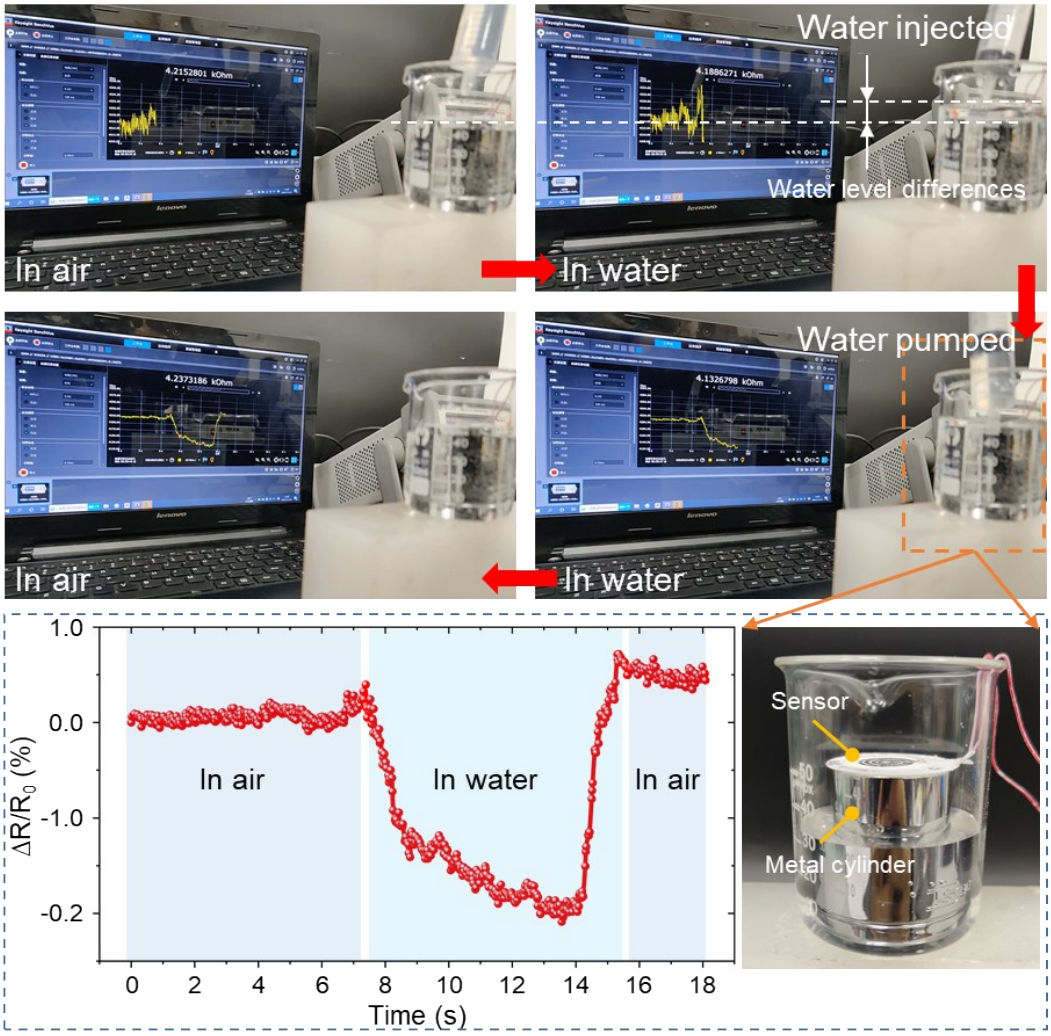

Fig. S13. The waterproof function test of sensor in air/water and underwater. The relative resistance change of sensor when immersed underwater. The sensor was fixed on top of a metal cylinder and placed together in a beaker. Water was injected into the beaker until the sensor was immersed, and then water was pumped away until the sensor was exposed to the air.

Supplementary Tables

Table S1 Comparison of the properties of the paper or polymer-based sensor in the references and that in our work

Materials	Fabricating methods	Sensor type	Mechanical signal	Stability	Superhydrophobicity	Sensivity	Working range	Other performances	Ref
Tissue paper/AuNWs/PDMS	Dip-coating	Resistant	Pressure/Strain	50,000	✗	P: > 1.14 kPa^{-1} S: 7.38 (0~14%); 1.82 (14~25%)	P:13~50,000Pa; S:0~25%	Power consumption of <30 μW	[1]
Carbonized tissue paper/PDMS	Pyrolysis	Resistant	Strain	1000	✗	S: 25.3 (0~3%); 4.73 (3~20%)	S:0~20%	Elongation at break: ~228%	[2]
CB/Filter paper/CMC	Dip-coating	Resistant	Strain	1000	✗	S: 4.3 (0~0.6%)	S:0~0.6%	Responsive time: ~240 ms	[3]
A4 paper/Graphite	Paper-remaking/mixing	Resistant	Strain	1000	✗	S: 10.5 (0~24%); 27.0 (0.24~0.73%)	S:0~2.1%	Response time: ~ 440 m	[4]
Carbonized tissue paper/PDMS	Pyrolysis	Resistant	Strain	10000	✗	S: 10.1 (0–1.35%)	S:-5~5%	Response time: <115 ms	[5]
A4 paper/Mexne	Depositing	Resistant	Strain	1000	WA: 157°; CA: 4.5°	S: 17.4 (0–0.6%)	S:0~0.8%	Response time: (200 ms); Detection limit (0.1% strain)	[6]
Tissue paper/Graphene/	Soaking	Resistant	Pressure	300	✗	P:17.2 kPa^{-1} (0~2 kPa); 0.1 kPa^{-1} (2~20 kPa)	P: 0~20 kPa	-	[7]
Printig paper/CB/MWCNTs/MC	Dip-coating	Resistant	Strain	1000	WA: 154°; CA: -	S: 7.5 (0~0.7%)	S:-0.7~0.7%	Ultralow strain as low as 0.1%	[8]
PDMS/Au-(based on groove structure)	Mold, sputter-coating	Resistant	Strain	10000	✗	S: 2557.71	S:0~45%	Response time: <130 ms; Detection limit: 0.1% strain	[9]
SEBS/CNTs-(based on groove structure)	Extruding, ultrasonic treatment	Resistant	Strain	2000	✗	S: 0.12 (0~90%); 17.36 (90~240%)	S:0~240%	Response time: <300 ms	[10]
PDMS/SCF/CNT-(based on groove structure)	Mold, hot-embossing	Resistant	Pressure	1000	✗	P:6.3 kPa^{-1} (0~0.125 kPa)	P: 0~0.35 kPa	-	[11]
Photo paper/Ag/MWCNTs/SiO_2/PDMS	**Spray coating**	**Resistant**	**Pressure/Strain**	**700/1 hour**	**WA: 152.3°; CA: 7.3°**	**P: 0.43%kPa^{-1} (0~100 kPa), 0.18%kPa^{-1} (100~160 kPa); S: 40 (0~0.05%); 1.82 (0.05~0.12%)**	**P:0~190 kPa; S:0~0.12%**	**Strain resolution: 0.003%**	**Our work**

References:

1 S. Gong, W. Schwalb, Y. Wang, Y. Chen, Y. Tang, J. Si, B. Shirinzadeh and W. Cheng, *Nat. Commun.*, 2014, **5**, 3132.

2 Y. Li, Y. A. Samad, T. Taha, G. Cai, S. Y. Fu and K. Liao, *ACS Sustain. Chem. Eng.*, 2016, **4**, 4288-4295.

3 H. Liu, H. Jiang, F. Du, D. Zhang, Z. Li and H. Zhou, *ACS Sustain. Chem. Eng.*, 2017, **5**, 10538-10543.

4 H. Liu, H. Xiang, Y. Ma, Z. Li, Q. Meng, H. Jiang, H. Wu, P. Li, H. Zhou and W. Huang, *ACS Sustain. Chem. Eng.*, 2018, **6**, 15749-15755.

5 S. Chen, Y. Song, D. Ding, Z. Ling and F. Xu, *Adv. Funct. Mater.*, 2018, **28**, 1802547.

6 Y. Bu, T. Shen, W. Yang, S. Yang, Y. Zhao, H. Liu, Y. Zheng, C. Liu and C. Shen, *Sci. Bull.*, 2021, **66**, 1849-1857.

7 L. Tao, K. Zhang, H. Tian, Y. Liu, D. Wang, Y. Chen, Y. Yang and T. Ren, *ACS Nano*, 2017, **11**, 8790-8795.

8 Q. Li, H. Liu, S. Zhang, D. Zhang, X. Liu, Y. He, L. Mi, J. Zhang, C. Liu, C. Shen and Z. Guo, *ACS Appl. Mater. Interfaces*, 2019, **11**, 21904-21914.

9 J. Ji, C. Zhang, S. Yang, Y. Liu, J. Wang and Z. Shi, *ACS Appl. Mater. Interfaces*, 2022, **14**, 24059-24066.

10 X. Cui, Y. Jiang, Z. Xu, M. Xi, Y. Jiang, P. Song, Y. Zhao and H. Wang, *Compos. Part B Eng.*, 2021, **211**, 108641.

11 X. Bai, C. Gai, D. Wu, J. Zhu, G. Wu, M. Zhang, Y. Liu, J. Sun, J. Zhuang, Y. Huang and H. Xu, *IEEE Sens. J.*, 2022, **22**, 3113-3121.